Journal of Applied Polymer Science

Ethylene–Propylene-Diene Terpolymer/Halloysite Nanocomposites: Thermal, Mechanical Properties, and Foam Processing

Kangsuk Lee,[1] Young-Wook Chang,[1] Seong Woo Kim[2]
[1]Department of Chemical Engineering, Hanyang University, Ansan 426-791, Korea
[2]Department of Chemical Engineering, Kyonggi University, Suwon 443-760, Korea
Correspondence to: Y.-W. Chang (E-mail: ywchang@hanyang.ac.kr)

ABSTRACT: Ethylene–propylene-diene terpolymer (EPDM)/halloysite nanotube (HNT) nanocomposites were prepared by melt mixing in an internal mixer using a commercially available maleated semicrystalline EPDM and HNT. Transmission electron microscopy analysis of the EPDM/HNT composites revealed that the HNTs are uniformly dispersed at a nanometer scale in the matrix. Differential scanning calorimeter studies indicated that the HNT caused an increase in the nonisothermal crystallization temperature of the EPDM. Tensile and dynamic mechanical analysis exhibited that a small amount of the HNTs effectively enhanced the stiffness of the EPDM without adversely affecting its elongation-at-break. The EPDM/HNT nanocomposites were used to produce foams by using a batch process in an autoclave, with supercritical carbon dioxide as a foaming agent. The nanocomposite foams showed a smaller cell size and higher cell density as compared to the neat EPDM foam, and the nanocomposite with 10 phr HNT produced a microcellular foam with average cell size as small as 7.8 μm and cell density as high as 1.5×10^{10} cell/cm^3. © 2013 Wiley Periodicals, Inc. J. Appl. Polym. Sci. **2014**, *131*, 40307.

KEYWORDS: elastomers; composites; foams

Received 4 October 2013; accepted 15 December 2013
DOI: 10.1002/app.40307

INTRODUCTION

Polymer nanocomposites with inorganic nanoparticles have been regarded as an important class of materials. The nanocomposites exhibit greatly improved physical and mechanical properties or new functional properties at relatively low inorganic filler loading levels as compared to the conventional microcomposites.[1–4] The enhanced properties are because of the huge interfacial areas and a resultant interfacial interactions between the nanosized fillers and polymer chains. Various types of nanofillers with spherical, layered, or fibrous shapes involving nanosilica, layered silicate clay, carbon nanotube, and cellulose nanowhiskers have been employed to prepare the polymer nanocomposites.

Recently, studies on the preparation of microcellular foam based on the polymer nanocomposites have been conducted. It has been found that the nanoparticles in polymer matrix serve as efficient nucleation agents by reducing the nucleating energy for the formation of nucleation centers because of their extremely fine dimensions with large surface area and intimate contact between the nanoparticles and the matrix polymer.[5–12]

Halloysite nanotube (HNT), a type of naturally occurring clay mineral with a chemical composition similar to kaolin having chemical formula $Al_2Si_2O_5(OH)_4{\cdot}2H_2O$, has a tubular structure resembling carbon nanotubes with a high length-to-diameter ratio (L/D) and is attracting interest as a new class of nanofiller to reinforce polymers. Typically, the size of HNT nanoparticles varies from 50 to 70 nm in external diameter and 100–2000 nm in length, with about a 15 nm diameter lumen. The nanorod-like geometry of HNT is not intertwined like CNT or not interlinked like layered silicates which allows the HNT dispersion in the polymer matrix to be easier than CNT and layered silicates.[13–15] It has been reported that the HNTs confer enhanced mechanical properties, thermal stability, and anti-flammability characteristics to various thermoplastics like nylon,[16] polycaprolatone,[17] polyethylene,[18] polypropylene,[19–21] and rubber valcanizates like Ethylene–propylene-diene terpolymer (EPDM)[22,23] and SBR.[24,25] It has been reported that nanoscaled dispersion of the HNT in nonpolar polyolefins can be obtained when a proper compatibilizer is added or the matrix polymer is modified with polar functional group like carboxylic acid.[20,22,24,25]

EPDM is an important elastomer widely used in applications such as automotive parts, durable goods, wire and cable owing to its outstanding heat, ozone and weather resistance, and excellent electrical insulating properties. There have been extensive studies on the EPDM nanocomposite vulcanizates with organoclay.[26–32]

However, studies on EPDM/HNT nanocomposites are rare[22,23] and on the foams thereof have not been reported.

In this study, we prepared the nanocomposite using a commercially available maleic anhydride grafted semicrystalline EPDM with HNT via melt blending method, and their thermal, mechanical properties and the possibility of fabrication of microcellular foam with the nanocomposite using supercritical carbon dioxide as a blowing agent was investigated.

EXPERIMENTAL

Materials

Commercially available maleated semicrystalline EPDM (Royaltuf 485) was purchased from Crompton (Seoul, Korea). It has an ethylene/propylene ratio of 75/25, 0.5 wt % maleic anhydride functionality and 4.9 wt % of ENB. The tubular HNT shown in Figure 1 was purchased from Aldrich and was used without any chemical modification. The HNT has specific gravity of 2.53, surface area of 64 m^2/g, pore volume of 1.26–1.34 mL/g, cation exchange capacity of 8.0 meq/g, and Zeta potential of −22.543 mV.

Preparation of Nanocomposite

EPDM and HNTs were dried under vacuum (30 in Hg) at 50°C for 5 hr before use. The composites were prepared by melt blending in an internal mixer (Haake Polylab 600) using a rotor speed of 60 rpm and at a temperature of 150°C for 10 min. The amount of HNT was 3, 5, 7, and 10 parts per hundred resin (phr). The obtained compounds were compression molded as sheet of 1 mm thickness at 150°C for 10 min under a pressure of 13 MPa using an electrically heated hydraulic press (Carver, USA).

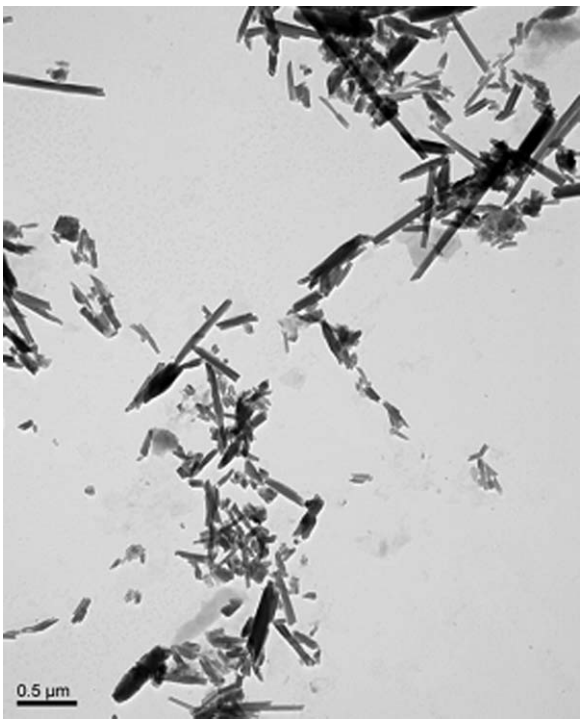

Figure 1. TEM micrograph of HNTs used in this study.

Foam Processing

The polymer sample of 1 mm thick was first placed in an autoclave connected to a carbon dioxide cylinder. The system was then saturated with carbon dioxide for 24 hr to allow the CO_2 saturation and equilibrium at a predetermined foaming temperature (130°C) and pressure (30 MPa).[12] The pressure was released by opening the pressure value. The decompression was found to be completed in 10 sec. The system was maintained at atmospheric pressure for approximately 1 hr so that the bubbles could grow completely, and the foam was cooled with an ice and water mixture to fix the morphology.

Characterizations

Dispersion of the HNTs in the EPDM/HNT composite was evaluated using transmission electron microscopy (TEM). TEM micrographs were obtained with a JEOL 200CX TEM using an acceleration voltage of 200 kV.

X-ray photoelectron spectroscopy (XPS) spectra of neat mEPDM and mEPDM/HNT nanocomposites were recorded by using an X-ray photoelectron spectrometer (K-Alpha, Thermo Fisher Scientific, MA, USA) with Aluminum (mono) Ka X-ray source (1486.6 eV) operated at 15 kV voltage and 10 mA current. The high-resolution survey was performed for all the samples at spectral regions related to carbon and oxygen atoms.

Nonisothermal crystallization and melting temperatures of samples were determined using a differential scanning calorimeter (TA Instrument DSC 2010). 10 mg of the samples dried completely in vacuum oven was used for the analysis. It was heated from 30°C to 160°C at a rate of 10°C/min under a nitrogen atmosphere and was kept for 10 min at this temperature to remove thermal history. Then, the sample was cooled to 30°C at a rate of 10°C/min to induce nonisothermal crystallization. The nonisothermally melt crystallized sample was heated again to 160°C at a rate of 10°C/min to observe melting behavior.

The ultimate tensile strength, elongation at break, and tensile moduli were determined using a universal testing machine (United, STM-10E) at 25°C and with a crosshead speed of 500 mm/min, according to ASTM D412 specifications. Tension set was measured to evaluate the elastic recoverability of the samples by stretching the specimen to 100% elongation and keeping them in that position for 10 min. The applied stress was then released and the specimen was kept for 10 min. Tension set was determined by the following formula:

$$\text{Tension set } (\%) = (\text{change in length} / \text{original length}) \times 100$$

Tear strength was measured as per ASTMD 624 using un-nicked 90° angle test pieces (die C) at 25°C at a crosshead speed of 500 mm/min using a universal testing machine (United, STM-10E). And, the tear fracture surface was examined using scanning electron microscope (SEM, Jeol 1100).

Dynamic mechanical properties were measured using a dynamic mechanical analyzer (TA instrument DMA 2980). The sample was subjected to a cyclic tensile strain with an amplitude of 0.2% and a frequency of 10 Hz. The temperature was increased at a heating rate of 2°C/min from −100°C to 200°C.

Thermogravimetric analysis (TGA) was conducted with a thermogravimetric analyzer (SDT 2960, TA Instruments) under nitrogen atmosphere with a flow rate of 50 mL/min. The temperature was increased at a heating rate of 10°C/min from 30°C to 800°C.

For the observation of cell structure of the foamed samples, they were fractured using liquid nitrogen and sputter coated with gold and were examined by scanning electron microscopy (SEM, Jeol 1100). The mass density of both original sample (ρ_p) and foamed sample (ρ_f) in g/mL was estimated by using the method of buoyancy. The average cell size d in μm was determined from the SEM images. The cell densities of the foamed samples (N_c) in cell/cm^3 and mean cell wall thickness δ in μm were determined by using the following equations[11,12]:

$$N_c = 10^4\left[1 - \left(\rho_f/\rho_p\right)\right]/d^3 \quad (1)$$

$$\delta = d\left[1/\left(1 - \left(\rho_f/\rho_p\right)\right)^{0.5} - 1\right] \quad (2)$$

The compressive modulus (CM) of foam samples were measured using a universal testing machine (United, STM-10E) at 25°C. The specimens had dimensions of 20 × 20 × 2.5 mm and the crosshead speed of compression was set at 1 mm/min.

RESULTS AND DISCUSSION

Structure of EPDM/HNT

The degree of dispersion of the clay nanoparticles can be directly seen in TEM photographs of ultrathin section of a compression-molded EPDM nanocomposite with HNT loading of 3, 5, 7, and 10 phr, which are shown in Figure 2. It is apparent that the individually separated HNTs, about 50–70 nm in diameter, are uniformly dispersed in the matrix polymer and some aggregated HNTs coexist in the samples with high loadings of the HNTs. The TEM photographs also show that the HNTs are randomly oriented. It should be noted that the integrity of the nanotubes is destroyed when the nanocomposite samples are cut using an ultra-microtome. The nano-scaled dispersion of HNTs indicates that there is a certain extent of compatibility between the surface of the HNT and maleated EPDM chains.

Specific Interactions in EPDM/HNT

The XPS analysis are often used to examine the specific interactions between the filler and matrix polymer in polymer nanocomposites as the binding energy of a core-level electron depends on its chemical environment.[17,33,34] The XPS spectra of carbon and oxygen atom of EPDM in neat EPDM and EPDM/HNT nanocomposites are shown in Figure 3(a) and (b),

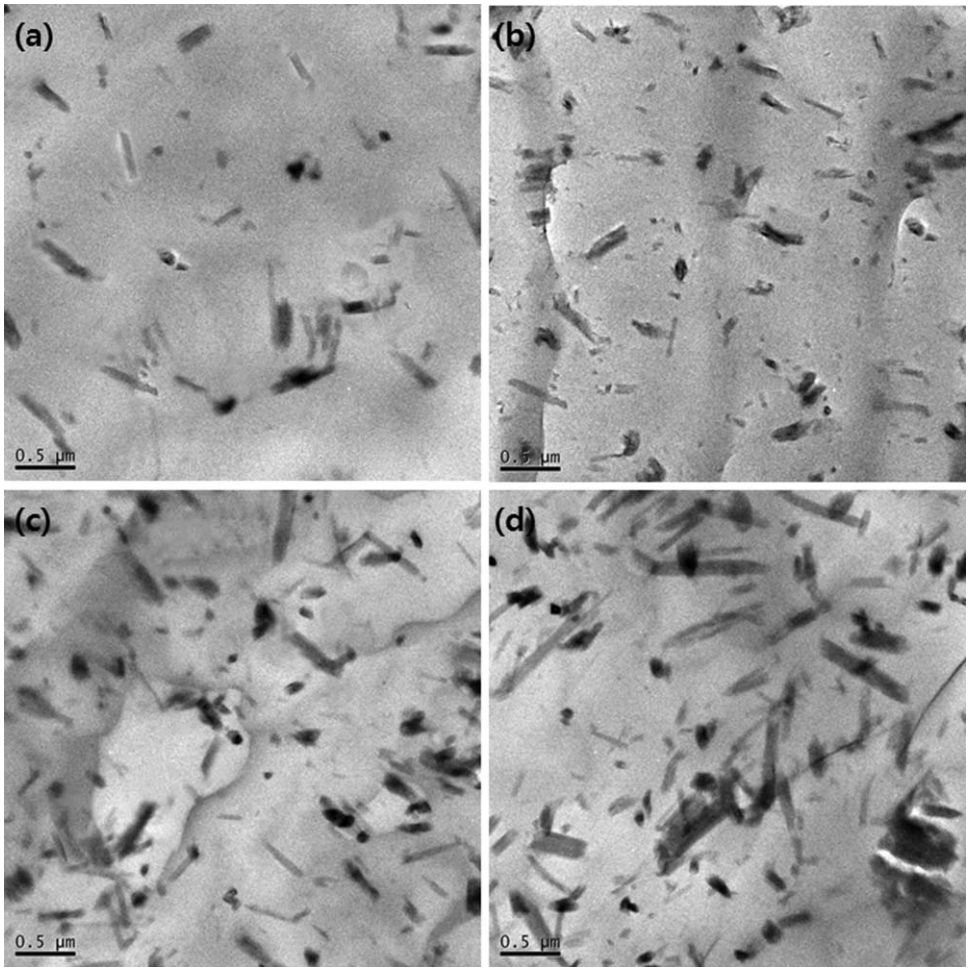

Figure 2. TEM images of EPDM/HNT nanocomposites with different HNT loadings: (a) 3 phr, (b) 5 phr, (c) 7 phr, and (d) 10 phr.

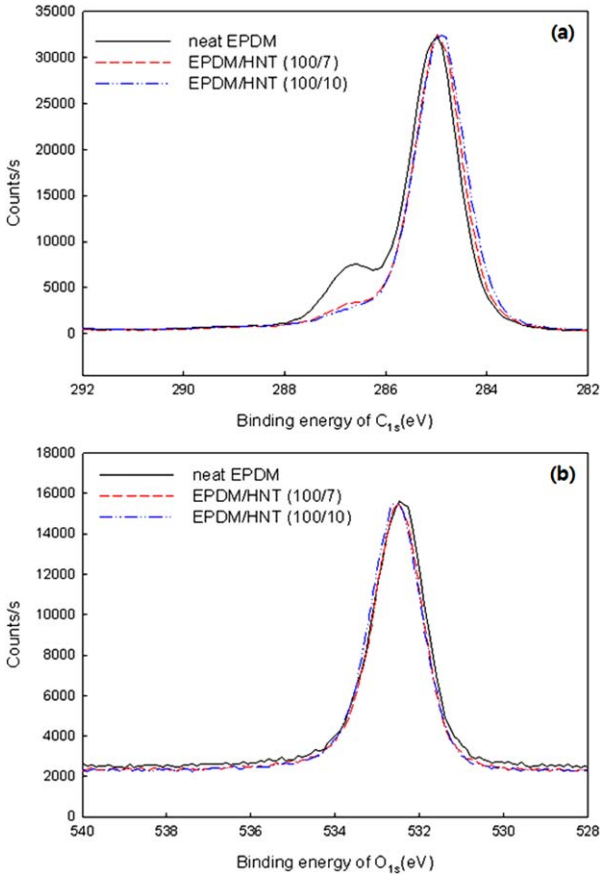

Figure 3. XPS spectra of neat EPDM and EPDM/HNT nanocomposites: (a) C_{1s} and (b) O_{1s}. [Color figure can be viewed in the online issue, which is available at wileyonlinelibrary.com.]

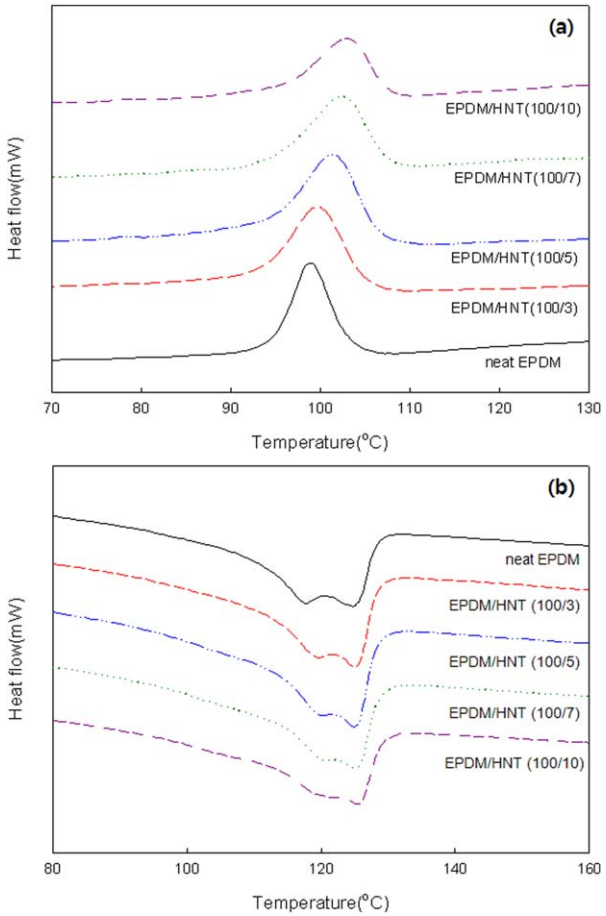

Figure 4. DSC thermograms of neat EPDM and EPDM/HNT nanocomposites: (a) Crystallization exotherms and (b) melting endotherms. [Color figure can be viewed in the online issue, which is available at wileyonlinelibrary.com.]

respectively. The binding energy for carbon atom (C_{1s}) is reduced from 285.05 for neat EPDM to 284.92 eV for EPDM/HNT (100/10) nanocomposite. Furthermore, the binding energy for oxygen atom (O_{1s}) is changed from 532.40 for neat EPDM to 532.55 eV for EPDM/HNT (100/10) nanocomposite. These changes in the binding energy of the atoms are attributed to the presence of hydrogen bonding between the hydroxyl group (−OH) present on the HNT surface and carbonyl group of the maleated EPDM chains.[17,22]

Crystallization and Melting Behavior

EPDM employed in this study has a certain degree of crystallinity. Effects of HNT on the crystallization and melting behavior of the samples were examined using DSC. DSC thermograms of nonisothermal crystallization and re-melting process for neat EPDM and EPDM/HNT nanocomposites are shown in Figure 4(a) and (b), respectively, and the thermal transition parameters are summarized in Table I. In the cooling process of DSC measurement, the nanocomposites show higher crystallization peak temperatures (T_c) than neat EPDM. With 5 phr HNT, the T_c is increased by 2.5°C and it increased with further addition of the HNT. The increase in T_c indicates an increased crystallization rate in the nanocomposites. An increase in the crystallization rate has also been observed in other semicrystalline polymer/HNT nanocomposites, in which HNT nanolayers can adsorb polymer chains more easily and the HNT particles act as nucleating agents.[16,21] In the remelting processes, shown in Figure 4(b), both neat EPDM and its nanocomposites show double melting behavior, indicating that two different types of crystalline structure exists in the polymer.

Mechanical Properties

Reinforcement effects in the EPDM/HNT nanocomposites were examined by tensile and dynamic mechanical measurement. Table II presents the moduli at given strains, tensile strength, and elongation-at-break determined from stress–strain curves, along with the tension set and tear strength values. It is observed that tensile modulus and strength increased with increasing HNT

Table I. DSC Data of Neat EPDM and EPDM/HNT Nanocomposites

HNT contents (phr)	T_c (°C)	ΔH_c (J/g)	T_{m1} (°C)	T_{m2} (°C)
0	98.9	10.1	118.0	124.8
3	100.5	10.2	118.9	125.0
5	101.4	10.1	119.4	125.2
7	102.6	10.0	119.9	125.4
10	103.8	10.2	120.5	125.5

Table II. Tensile Properties and Tear Strength of Neat EPDM and EPDM/HNT Nanocomposites

HNT contents (phr)	Modulus at a given extension (MPa)			Tensile strength (MPa)	Elongation-at-break (%)	Tension set (%)	Tear strength (kN/m)
	50%	100%	300%				
0	1.08 ± 0.1	1.35 ± 0.2	1.66 ± 0.2	1.91 ± 0.2	649±20	6.2±0.1	33.8±0.5
3	1.33 ± 0.1	1.61 ± 0.2	1.94 ± 0.2	2.04 ± 0.3	672 ± 22	7.8 ± 0.1	37.7 ± 0.6
5	1.46 ± 0.2	1.84 ± 0.2	2.14 ± 0.3	2.21 ± 0.3	661 ± 20	9.2 ± 0.2	41.3 ± 0.6
7	1.49 ± 0.2	1.89 ± 0.2	2.29 ± 0.3	2.21 ± 0.3	642 ± 20	10.5 ± 0.2	46.4 ± 0.7
10	1.71 ± 0.2	2.06 ± 0.3	2.44 ± 0.3	2.49 ± 0.3	626 ± 18	11.8 ± 0.2	48.4 ± 0.7

content. For example, 100%, 300% modulus, and tensile strength of the EPDM/HNT(100/5) nanocomposite increased by about 36%, 29%, and 16% as compared to those of neat EPDM, respectively. It is also to be noted that the increase in the modulus and strength in the nanocomposites is accompanied by retention of elongation-at-break of neat EPDM. Similar trends in the tensile behavior were also observed in EPDM/HNT nanocomposite vulcanizates[22,23] as well as other elastomer/organoclay nanocomposites such as polyurethane/organoclay nanocomposites[35,36] and SEBS/organoclay nanocomposite.[37] This is in contrast with the tensile behavior of conventional elastomer composites containing micron-sized inorganic fillers, in which the enhanced modulus is typically accompanied with sacrificing the elongation-at-break. The mechanism for the unique tensile behavior in the nanocomposites is not clear at present. It is proposed that huge interfacial interactions between the matrix polymer and inorganic nanoparticles contribute to the unique behavior.

Tear test was performed to examine the effect of HNT on the failure mode of the matrix EPDM. It can be seen that the tear strength, a measure of resistance to crack propagation, increased with increasing HNT content. With 5 and 10 phr HNT, the tear strength increased by about 22% and 43%, respectively, as compared to neat EPDM. This indicates that the uniformly dispersed HNTs act as physical barriers against a growing crack, which leads to the increase in the resistance to tearing of the matrix rubber. SEM photos of the tear fracture surfaces presented in Figure 5 show that the fracture surface become rougher with increasing HNT content in the nanocomposites, which reveal that crack growth is effectively hindered by HNT dispersed in the matrix rubber.

Tension set was measured to evaluate the elastic recoverability of the samples. It can be seen that the tension set value of neat EPDM is about 5%, revealing that it is highly elastic. The tension set increases with HNT content in the nanocomposites, but all the nanocomposites show the tension set value less than 12%, indicating that the nanocomposites studied here have good elastic recoverability.

Reinforcing effect of the HNT can also be seen from the temperature dependence of dynamic storage moduli (E') of the samples. It can be seen that EPDM/HNT nanocomposites exhibited higher storage modulus than neat EPDM over the entire temperature range and the storage modulus increased with increasing HNT content in the nanocomposites. The value of E' at 30°C, 100°C, and 150°C as well as the glass transition temperature are listed in Table III. The E' at 30°C and 150°C showed an increasing trend from 0 to 10 phr HNT loading by a factor 1.5 and 2.1, respectively, indicating that the HNT dispersed in the semicrystalline EPDM matrix enable the matrix polymer to sustain a high modulus value at higher temperature. Such an effective modulus enhancement on the addition of small amount of clay particles in the nanocomposite is attributed to the huge interfacial areas between the polymer and nanoscaled dispersed HNTs.

Thermal Stability

Thermal stability of the EPDM/HNT nanocomposites was examined using TGA and the results are summarized in Table IV. The results show that the thermal stability of the EPDM is increased by HNT. At 10 wt % HNT, the temperature at 5% and 10% weight loss are increased by about 35°C and 22°C compared to neat EPDM, respectively. A similar increase in thermal stability has been reported in other polymer/HNT nanocomposites. The increased thermal stability is attributed to the entrapment of degradation products of the matrix polymers inside the lumens HNTs, resulting in effective delay in mass transport.[16,19,23]

Foam Processing, Cellular Structure, and Foam Properties

Figure 6 shows the results of SEM images of the freeze-fracture surfaces of the neat EPDM foam and EPDM/HNT nanocomposites foams. Various morphological parameters of the foams were obtained from the SEM images and the results are summarized in Table V, along with foam density and compressive moduli of the foams. It can be seen that EPDM/HNT nanocomposite foams have lower average cell size and higher cell density than neat EPDM foam. With increasing HNT content from 0 to 10 phr, cell size is reduced from 12 to 7.8 μm, and the cell density increases to 1.5×10^{10} cell/cm^3, about 3.7 times larger than that of the neat EPDM foam. In addition, the cell wall thickness decreased from 2.06 μm for neat EPDM foam to 1.62 μm for the nanocomposite with 10 phr HNT. These results revealed that HNTs dispersed at nanometer scale in matrix EPDM act as effective nucleating agents for the foaming process, and effective increase in the modulus because of HNTs in the nanocomposite may restrain growth of cells and their coalescence, resulting in the reduction in the cell size of the foam as compared to the neat EPDM foam. It is also to be noted that EPDM/HNT nanocomposite foams show higher CM than neat EPDM foam, which are because of small cell size and high cell density of the nanocomposite foams.

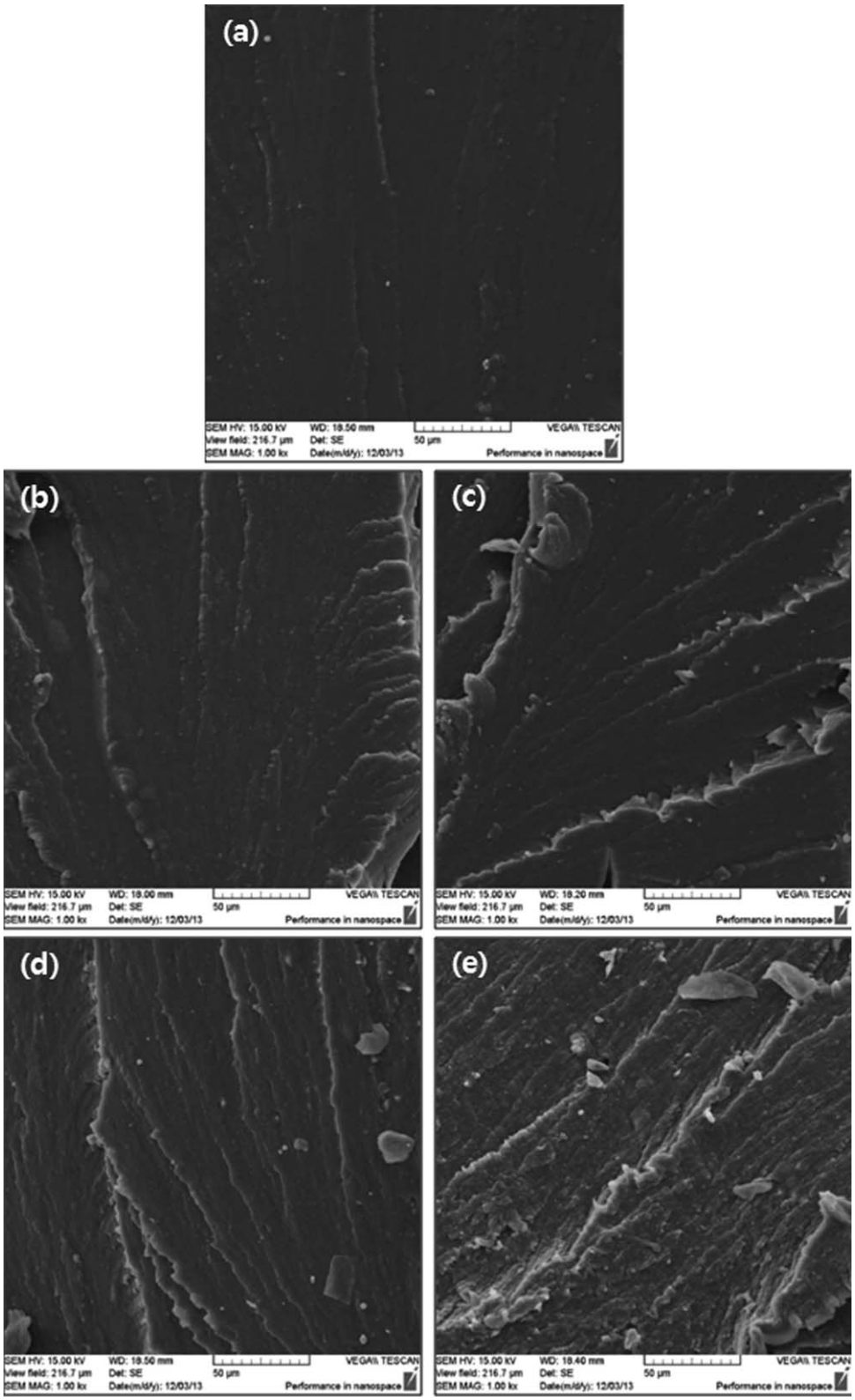

Figure 5. SEM images of tear fracture surface of (a) neat EPDM and (b)–(e) EPDM/HNT nanocomposites with different HNT loadings (b) 3 phr, (c) 5 phr, (d) 7 phr, and (e) 10 phr.

Table III. Dynamic Storage Moduli of Neat EPDM and EPDM/HNT Nanocomposites at Various Temperatures and Their Glass Transition Temperatures Obtained from Tan δ Peak

HNT contents (phr)	Storage modulus (MPa)			Glass transition temperature(°C)
	30°C	100°C	150°C	
0	13.5	1.39	0.43	−32.4
3	13.9	1.59	0.54	−32.0
5	16.1	1.80	0.61	−31.1
7	18.1	2.17	0.81	−31.2
10	20.7	2.71	0.89	−31.6

Table IV. TGA Data of Neat EPDM and EPDM/HNT Nanocomposites

HNT content (phr)	Temperature at 5% weight loss (°C)	Temperature at 10% weight loss (°C)	Char yield (wt %)
0	352.2	374.1	0.0
3	370.4	381.0	2.7
5	385.3	394.3	4.4
7	386.6	395.4	6.3
10	387.2	396.2	8.7

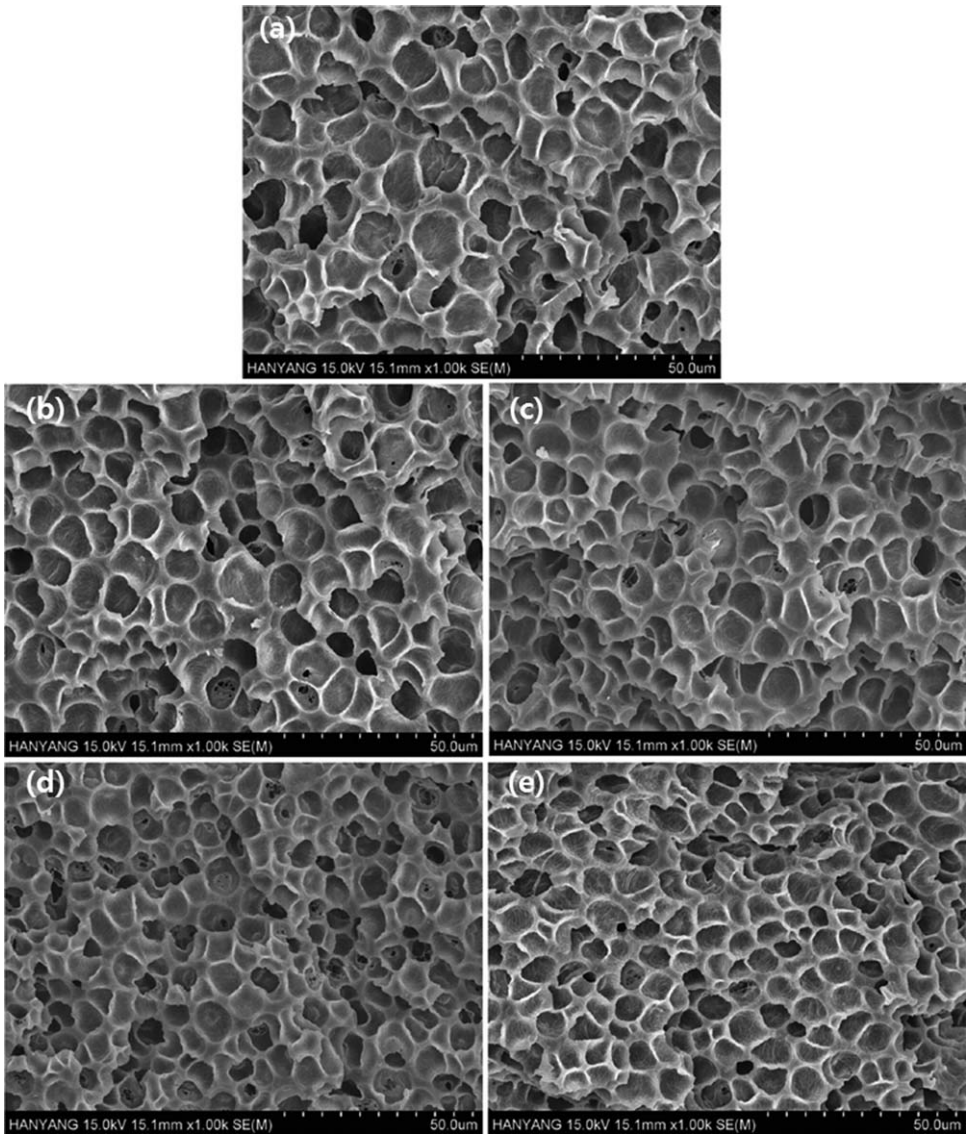

Figure 6. SEM images of the freeze-fracture surface of (a) neat EPDM foam and (b)–(e) EPDM/HNT nanocomposite foams with different HNT loadings: (b) 3 phr, (c) 5 phr, (d) 7 phr, and (e) 10 phr.

Table V. Density, Morphological Parameters and Compressive Modulus of Neat EPDM Foam and EPDM/HNT Nanocomposite Foams

HNT contents (phr)	ρ_f (g/cm^3)	d (μm)	N_c (cell/cm^3)	δ (μm)	CM (MPa)
0	0.23	12.0	4.21×10^9	2.06	1.80 ± 0.05
3	0.35	10.8	4.79×10^9	3.11	2.15 ± 0.06
5	0.34	9.2	7.95×10^9	2.50	2.28 ± 0.06
7	0.32	8.4	1.09×10^{10}	2.04	2.35 ± 0.05
10	0.29	7.8	1.54×10^{10}	1.62	2.43 ± 0.05

CONCLUSIONS

Nanocomposites could be fabricated by melt blending of semicrystalline EPDM grafted with a small amount of maleic anhydride and HNT in an internal mixer. Tensile, dynamic mechanical analysis, and DSC measurements revealed that the HNTs act as effective reinforcing fillers and nucleating agents for nonisothermal crystallization process for the matrix rubber without sacrificing its rubber-like properties. And, it was found that the nanocomposite can produce a microcellular foam with average cell size as small as 7.8 μm and cell density as high as 1.5×10^{10} cell/cm^3 when the foaming was processed in supercritical CO_2, revealing that the HNTs act as effective nucleating agent for the foaming process. Such microcellular elastomeric nanocomposite foam can be potentially used in a variety of industrial applications involving gaskets and seals for automotives and electrical enclosures.

ACKNOWLEDGMENT

This work was supported by the National Research Foundation of Korea (NRF) grant funded by the Korea government (MSIP) (NO.2005-0049406).

REFERENCES

1. Giannelis, E. P. *Adv. Mater.* **1996**, *8*, 29.
2. Moniruzzaman, M.; Winey, K. L. *Macromolecules* **2006**, *39*, 5194.
3. Paul, D. R.; Robeson, L. M. *Polymer* **2008**, *49*, 3187.
4. Zou, H.; Wu, S.; Shen, J. *Chem. Rev.* **2008**, *108*, 3893.
5. Chen, L.; Rende, D.; Schadler, L. S.; Ozisik, R. *J. Mater. Chem. A.* **2013**, *1*, 3837.
6. Li, Y.; Ren, H.; Ragauskas, A. J. *J. Nanosci. Nanotechnol.* **2011**, *11*, 6904.
7. Shen, J.; Zeng, C.; Lee, L. *J. Polymer* **2005**, *46*, 5218.
8. Zeng, C.; Han, X.; Lee, L. J.; Koelling, K. W. *Adv. Mater.* **2003**, *15*, 1743.
9. Mitsunaga, M.; Ito, Y.; Sinha Ray, S.; Okamoto, M.; Hirokawa, K. *Macromol. Mater. Eng.* **2003**, *288*, 543.
10. Zeng, C.; Hossieny, N.; Zhang, C.; Wang, B. *Polymer* **2010**, *51*, 655.
11. Zeng, C.; Han, X.; Lee, L. J.; Koelling, K. W. *Adv. Mater.* **2003**, *15*, 1743.
12. Chang, Y. -W.; Kim, S.; Bae, S.; Kang, S. C. *Kor. J. Chem. Eng.* **2011**, *28*, 1779.
13. Joussein, E.; Petit, S.; Churchman, J.; Theng, B.; Righi, D.; Delvaux, B. *Clay Miner.* **2005**, *40*, 383.
14. Shi, Y. -F.; Tian, Z.; Zhang, Y.; Shen, H. -B.; Jia, N. -Q. *Nanoscale Res. Lett.* **2011**, *6*, 608.
15. Du, M.; Guo, B.; Jia, D. *Polym. Int.* **2010**, *59*, 574.
16. Lecouvet, B.; Gutierrez, J. G.; Sclavons, M.; Bailly, C. *Polym. Degrad. Stab.* **2011**, *96*, 226.
17. Lee, K. S.; Chang, Y. -W. *J. Appl. Polym. Sci.* **2013**, *128*, 2807.
18. Zia, Z.; Luo, Y.; Guo, B.; Yang, B.; Du, M.; Jia, D. *Polym. Plast. Technol. Eng.* **2009**, *48*, 607.
19. Du, M.; Guo, B.; Jia, D. *Eur. Polym. J.* **2006**, *42*, 1362.
20. Liu, M.; Guo, B.; Lei, Y.; Du, M.; Jia, D. *Appl. Surf. Sci.* **2009**, *255*, 4961.
21. Ning, N.; Yin, Q.; Luo, F.; Zhang, Q.; Du, R.; Fu, Q. *Polymer* **2007**, *48*, 7374.
22. Pasbakhsh, P.; Ismail, H.; Ahmad Fauzi, M. N.; Abu Bakar, A. *Polym. Test.* **2009**, *28*, 548.
23. Ismail, H.; Pasbakhsh, P.; Ahmad Fauzi, M. N.; Abu Bakar, A. *Polym. Test.* **2008**, *27*, 841.
24. Du, M.; Guo, B.; Lei, Y.; Liu, M.; Jia, D. *Polymer* **2008**, *49*, 4871.
25. Lei, Y.; Tang, Z.; Zhu, L.; Guo, B.; Jia, D. *Polymer* **2011**, *52*, 2011.
26. Usuki, A.; Tukigase, A.; Kato, M. *Polymer* **2002**, *43*, 2185.
27. Zheng, H.; Zhang, Y.; Peng, Z.; Zhang, Y. *J. Appl. Polym. Sci.* **2004**, *92*, 638.
28. Da Silva, C., Haidar, B., Vidal, A., Miehe- -Brendle, J., Ledred, R.; Vidal, L. *J. Mater. Sci.* **2005**, *40*, 1813.
29. Ma, Y.; Wu, Y. -P.; Wang, Y. -Q.; Zhang, L. -Q. *J. Appl. Polym. Sci.* **2006**, *99*, 914.
30. Kang, D.; Kim, D.; Yoon, S. -H.; Kim, D.; Barry, C.; Mead, J. *Macromol. Mater. Eng.* **2007**, *292*, 329.
31. Li, P.; Yin, L.; Song, G.; Sun, J.; Wang, L.; Wang, H. *Appl. Clay Sci.* **2008**, *40*, 38.
32. Krajnc, M.; Karger-Kocsis, J.; Sebenik, U. *J. Appl. Polym. Sci.* **2013**, *127*, 950.
33. Zeng, R.; Rong, M. Z.; Zhang, M. Q.; Liang, H. C.; Zeng, H. M. *J. Mater. Sci. Lett.* **2001**, *20*, 1473.
34. Pucciariello, R.; Villani, V.; Langerame, F.; Gorrasi, G.; Vittoria, V. *J. Polym. Sci. B Polym. Phys.* **2004**, *42*, 3907.
35. Wang, Z.; Pinnavaia, T. *J. Chem. Mater.* **1998**, *10*, 3769.
36. Xu, R.; Manias, E.; Snyder, A. J.; Runt, J. *J. Biomed. Mater. Res.* **2003**, *64A*, 114.
37. Chang, Y. -W.; Shin, J. Y.; Ryu, S. H. *Polym. Int.* **2004**, *53*, 1047.